CrystEngComm

ROYAL SOCIETY OF CHEMISTRY

PAPER

View Article Online
View Journal | View Issue

Cite this: *CrystEngComm*, 2023, **25**, 1550

Synthesis of zirconium-based metal–organic frameworks with iron(II) clathrochelate ligands†

Suchetha Shetty,‡[ab] Karam B. Idrees, ‡[c] Haomiao Xie,[c] Bassam Alameddine *[ab] and Omar K. Farha*[cd]

Received 22nd December 2022,
Accepted 6th February 2023

DOI: 10.1039/d2ce01686a

rsc.li/crystengcomm

Zirconium-based metal organic frameworks (MOFs) are of great significance in supramolecular coordination chemistry, mainly as catalysts, due to their chemical stability and structural diversity. We report the synthesis of zirconium-clathrochelate based crystalline MOFs (**Zr-GU-1 to -4**) made from hexanuclear zirconium inorganic nodes and iron(II) clathrochelate-based ditopic carboxylic acid ligands bearing various lateral moieties, namely, butyl, cyclohexyl, phenyl and methyl groups. Among the various iron(II) clathrochelate linkers, the one with butyl side chains, *i.e.*, **Zr-GU-1**, forms stable crystalline MOFs as confirmed by single-crystal X-ray crystallography and exhibits a promising porosity with a BET surface area of ~650 m^2 g^{-1} after its activation with supercritical CO_2 ($ScCO_2$) from acetonitrile.

Introduction

Metal–organic frameworks (MOFs) are constructed from inorganic metal ions/metal clusters and organic ligands which are linked together by coordination bonds to form a well-defined framework in terms of both composition and structure.[1,2] Over the past few decades, the construction of metal–organic frameworks (MOFs) has been among the most promising and rapidly expanding fields in materials science due to the unique properties that they disclose, namely, their bottom-up synthesis which allows for making on-demand structures, excellent flexibility, and porous nature whose large specific surface bearing active sites can be adjusted.[3–5] With these unique properties, MOFs have found a myriad of applications across different fields, such as gas adsorption and separation,[6–8] chemical sensing,[9,10] catalysis,[11,12] lithium-ion batteries,[13,14] water treatment and biomedicine.[15,16] Recently, the preparation of MOFs has undergone a noticeable development by using multidentate aromatic carboxylic acid ligands as building blocks, due to their robustness and thermal stability.[17,18] Furthermore, these multidentate ligands can be easily deprotonated to balance the metal ion charge, without the need to include in the resulting framework lattice any additional uncoordinated counter-ions, which would occupy the channel voids and, consequently, block the MOFs pores.[19] These characteristics of the metal-carboxylate lattices are utilized in size- and shape-selective separations and catalysis.[20]

Reticular chemistry, whose rules allow for a rational design of MOFs to a great extent, has emerged as a powerful synthetic tool to alter the chemical composition, framework topology, porosity and its environment in porous crystalline materials.[21–23] By rationally choosing the target topologies and molecular building blocks, specific MOFs can be constructed with atomic precision.[24,25] Over the last few years, Zr-based MOFs have attracted great attention due to their exceptional chemical stability[26–33] and, besides the applications of these materials in various fields, among others, their use as catalysts for organic syntheses[34–36] and hydrolytic decontaminants of chemical warfare agents.[37–41] Herein, we report the synthesis of Zr-based MOFs employing octahedral iron(II) clathrochelate bearing ditopic carboxylic acid ligands and lateral butyl groups, affording readily stable crystalline MOFs at a low modulator concentration and exhibiting a high BET surface area reaching up to 650 m^2 g^{-1} after supercritical CO_2 ($ScCO_2$) activation from acetonitrile.

[a] *Department of Mathematics and Natural Sciences, Gulf University for Science and Technology, Kuwait. E-mail: alameddine.b@gust.edu.kw*
[b] *Functional Materials Group, Gulf University for Science and Technology, Kuwait*
[c] *Department of Chemistry and International Institute for Nanotechnology, Northwestern University, 2145 Sheridan Road, Evanston, Illinois 60208, USA. E-mail: o-farha@northwestern.edu*
[d] *Department of Chemical & Biological Engineering, Northwestern University, Evanston, Illinois 60208, USA*

† Electronic supplementary information (ESI) available: Fig. S1 (experimental PXRD patterns of **Zr-GU-3,4**); Fig. S2 (obtained crystal for **Zr-GU-2** for SCXRD analysis); Fig. S3 (comparative experimental PXRD patterns of **Zr-GU-1** synthesized, after $ScCO_2$ activation and DMF soaked post activation); Table S1 (crystal data and structure refinement for **Zr-GU-1**). CCDC 2224952. For ESI and crystallographic data in CIF or other electronic format see DOI: **https://doi.org/10.1039/d2ce01686a**

‡ S. S. and K. B. I. contributed equally to this work.

Materials synthesis and characterization

Materials

All reagents were obtained from commercial sources and used without further purification, unless otherwise noted.

X-ray diffraction analyses

Powder X-ray diffraction (PXRD) of MOFs was carried out at room temperature on a STOE-STADI MP powder diffractometer equipped with an asymmetric curved germanium monochromator (CuKα1 radiation, λ = 1.54056 Å) and a one-dimensional silicon strip detector (MYTHEN2 1K from DECTRIS). The line focused Cu X-ray tube was operated at 40 kV and 40 mA. The activated powder was sandwiched between two Kapton foils and measured in transmission geometry using a rotating holder. Intensity data from 1 to 40 degrees two theta were collected.

N_2 sorption measurements

N_2 adsorption and desorption isotherms on activated materials were measured at Northwestern University on an ASAP 2420 (Micromeritics) instrument at 77 K after activation. Ultra-high purity N_2 (99.999%) was purchased from Airgas and used as received. Sorption measurements were carried out using approximately 30–40 mg of the sample.

Supercritical CO_2 ($ScCO_2$) procedure

Supercritical CO_2 activation experiments were performed on a Tousimis Samdri PVT-30 critical point dryer. Before doing the $ScCO_2$ drying, the as-synthesized materials were soaked in DMF for 3 days, followed by solvent exchange into ethanol or acetonitrile for 1 day. The solvent was refreshed every 12 h, and 12 mL of fresh solvent was added into the vials. The material was then transferred to a small glass container with minimal solvent to cover the sample for $ScCO_2$ drying (note: do not let the materials dry in the solvent, and make sure the materials are always submerged in the solvent before performing the $ScCO_2$ drying procedure).

Single-crystal X-ray diffraction

SCXRD data were collected at 200 K, using a Rigaku Cu-Synergy diffractometer equipped with a shutterless electronic-noise free Hybrid Photon Counting (HPC) detector, a Cryostream 80–500 K (Cryostream Oxford Cryosystems, Oxford, United Kingdom), a CuKα (λ = 1.54184 Å) microfocus source with a beam size of ~110 μm, and a 4-circle Kappa geometry goniometer. The single crystals were mounted on a MicroMesh (MiTeGen) with paratone oil. The structures were determined by intrinsic phasing (SHELXT 2018/2) and refined by full-matrix least-squares refinement (SHELXL-2018/3) using the Olex2 software packages. The disordered non-coordinated solvents and alkane side chains were removed using the solvent marks option in the Olex2 software. The refinement results are summarized in Table S1.† Crystallographic data for **Zr-GU-1** in CIF format have been deposited in the Cambridge Crystallographic Data Centre (CCDC) under deposition number 2224952.

Synthesis of a Zr-clathrochelate MOF (Zr-GU-1)

A **Zr-GU-1** MOF was prepared solvothermally by combining a mixture of clathrochelate linker **GU-1** (0.0129 mmol, 11.9 mg) and $ZrOCl_2{\cdot}8H_2O$ (0.0155 mmol, 5.0 mg) in 1 mL DMF and 20 μL TFA at 120 °C for 48 h. The crystals were collected, washed three times over two days with anhydrous DMF and then sequentially immersed in anhydrous DMF.

Results and discussion

Previous reports have shown the synthesis of clathrochelate-based MOFs using copper or zinc metal nodes;[6,42,43] however, to the best of our knowledge, no crystal structures have been reported for iron(II) clathrochelate-based MOFs using zirconium nodes. Therefore, we attempted to synthesize the latter and obtain their single crystal structures by employing the iron(II) clathrochelate dicarboxylic acid linkers **GU-1 to -4**, as shown in Scheme 1, which were synthesized following a procedure reported in the literature[42] and bear different lateral groups, namely, butyl, cyclohexyl, phenyl and methyl moieties. **Zr-GU-1** MOF was synthesized solvothermally by mixing 12.9 μmol of **GU-1** (a linker with a soluble butyl chain) and $ZrOCl_2{\cdot}8H_2O$ (15.5 μmol) in 1 mL of DMF and 20 μL of TFA at 120 °C for 48 h. Similar conditions were used to prepare the Zr-clathrochelate MOFs **Zr-GU-2 to -4**, which bear various lateral chains on the linker (R = cyclohexyl, phenyl, or methyl). Although the MOF synthesis using the abovementioned linkers (**GU-2 to -4**) seems feasible, their lower solubility compared to **GU-1** required some additional

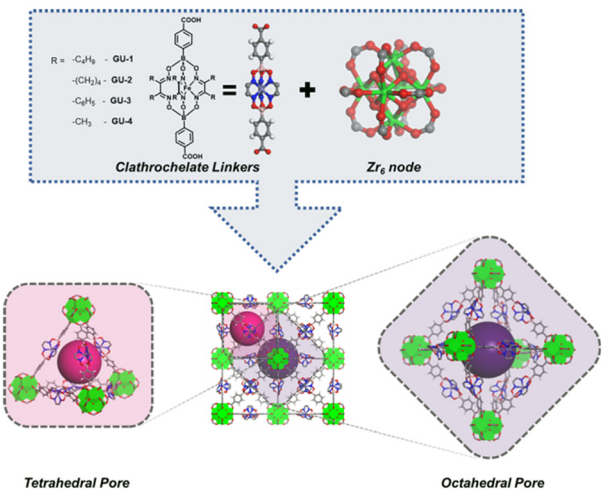

Scheme 1 Synthetic scheme of Zr-clathrochelate MOFs **Zr-GU-1 to -4** and formation of octahedral and tetrahedral cavities within the framework.

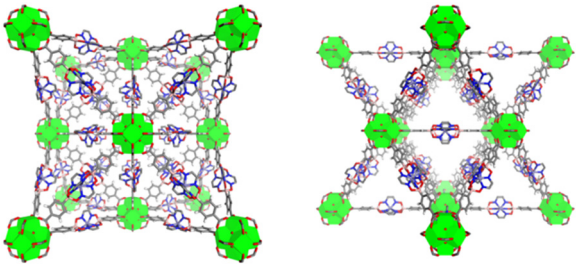

Fig. 1 SCXRD structure for **Zr-GU-1** along the *a*- and *b*-axis. Hydrogen atoms and disordered linkers are removed for clarity.

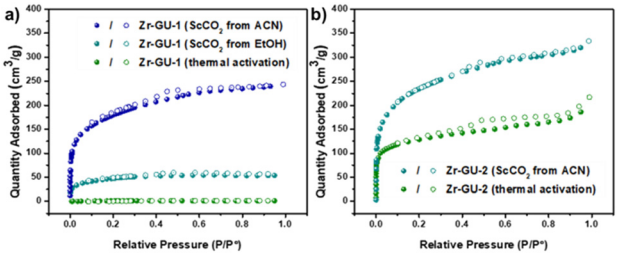

Fig. 3 Experimental N_2 adsorption and desorption isotherms at 77 K after $ScCO_2$ and thermal activation for (a) **Zr-GU-1** and (b) **Zr-GU-2**.

fine-tuning to obtain a crystalline sample of better quality (Fig. 2).

Interestingly, stable single crystals of **Zr-GU-1** with suitable sizes for SCXRD analysis were obtained by employing the synthetic conditions mentioned above. SCXRD data analysis revealed the atomic structure of **Zr-GU-1** which crystallizes in the $Fm\bar{3}m$ space group with an **fcu** topology (Fig. 1) and lattice constants $a = b = c = 37.5848(3)$ Å and $\alpha = \beta = \gamma = 90°$. **Zr-GU-1** is composed of hexanuclear zirconium (Zr_6) clusters bridged by ditopic iron(II) clathrochelate ligands to form both octahedral and tetrahedral cavities connected by triangular windows/pore apertures (Scheme 1). As could be noticed from Fig. 2, the as-synthesized and simulated powder X-ray diffraction (PXRD) patterns of **Zr-GU-1** are well-matched, thus confirming the phase purity of the bulk sample.

Several attempts were carried out to obtain SCXRD structures for the remaining MOFs **Zr-GU-2 to -4**. First, in order to overcome the low solubility of the clathrochelate linkers **GU-2 to -4**, we attempted a solvothermal synthesis of **Zr-GU-2 to -4** under the same conditions described above to make **Zr-GU-1** but employing a lower linker concentration of 2.9 μmol mmol instead of 12.9 μmol. These conditions were successful, affording large single crystals of **Zr-GU-2** but whose S CXRD structure was not feasible because the crystals decomposed soon after the removal of the solvent (Fig. S2†). Further efforts to obtain single crystals of **Zr-GU-3** and **Zr-GU-4** using other modulators such as acetic acid or formic acid were unsuccessful, and increasing the amount of the modulator resulted in the formation of different products as confirmed by PXRD analysis (Fig. S1†).

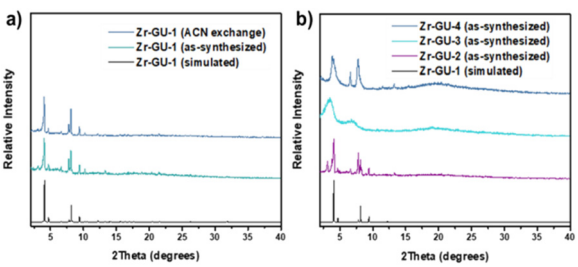

Fig. 2 (a) Experimental and simulated PXRD patterns of the as-synthesized **Zr-GU-1** and the following can exchange. (b) Comparison of the experimental PXRD patterns of **Zr-GU-2 to -4** with the simulated PXRD pattern of **Zr-GU-1**.

To probe the porosity of **Zr-GU-1**, we first tried thermal activation at 100 °C, but the N_2 adsorption isotherm at 77 K revealed no porosity. Therefore, an alternative attempt has been carried out by using supercritical CO_2 activation ($ScCO_2$) of **Zr-GU-1** from either ethanol (EtOH) or acetonitrile (ACN), where the latter exhibited the highest porosity obtained for **Zr-GU-1** compared to other activation methods with an experimental total pore volume of 0.37 $cm^3\ g^{-1}$ at $P/P^0 = 0.9$ compared to the theoretical pore volume of 0.83 $cm^3\ g^{-1}$. The apparent Brunauer–Emmett–Teller (BET) surface area of **Zr-GU-1** was found to be 650 $m^2\ g^{-1}$ (Fig. 3). It is noteworthy that the crystallinity of **Zr-GU-1** was lost following the $ScCO_2$ activation but was partially restored after soaking it back in ACN (Fig. S3†), therefore indicating a reversible structural change between the 'open' and 'closed' forms, which could be attributed to the lower experimental pore volume.

Due to the relatively high crystallinity of **Zr-GU-2** compared to **Zr-GU-3** and **Zr-GU-4**, we further investigated its bulk porosity using N_2 adsorption isotherms. Interestingly, **Zr-GU-2** exhibits significantly higher BET surface areas after thermal activation at 100 °C and $ScCO_2$ activation from ACN exchange compared to **Zr-GU-1**. The BET surface was found to be 475 $m^2\ g^{-1}$ after thermal activation compared to the negligible BET surface area for **Zr-GU-1** when using the same activation technique. Furthermore, $ScCO_2$ activation after ACN exchange yielded a BET surface area of 850 $m^2\ g^{-1}$ with a pore volume of 0.49 $cm^3\ g^{-1}$ (Fig. 3) compared to the theoretical pore volume of 0.91 $cm^3\ g^{-1}$. This larger BET surface area could mainly be attributed to the bulkier cyclohexyl lateral groups in **Zr-GU-2** which are positioned in close proximity to the framework walls, thus allowing the structure to maintain its 'open' form as opposed to the linear butyl groups in **Zr-GU-1**.

Conclusions

In summary, new metal organic frameworks (MOFs) based on zirconium were successfully synthesized using iron(II) clathrochelate-bearing ditopic carboxylic acid ligands and Zr_6 inorganic nodes. Stable crystalline MOFs were obtained from iron(II) clathrochelate based dicarboxylic acid linkers bearing lateral butyl groups **Zr-GU-1**, and their formation was confirmed by single-crystal X-ray crystallography. N_2-adsorption study of **Zr-GU-1** reveals a porous nature with a

pore volume of 0.37 cm^3 g^{-1}. Furthermore, the apparent Brunauer–Emmett–Teller (BET) surface area of **Zr-GU-1** was found to be 650 m^2 g^{-1} after acetonitrile $ScCO_2$ activation. Additionally, replacing the butyl groups with bulkier cyclohexyl groups allowed the framework to achieve a BET surface area of 850 m^2 g^{-1}.

Author contributions

Conceptualization, B. A. and O. F.; methodology, B. A. and O. F.; software, S. S., K. I., and H. X.; validation, H. X., B. A. and O. F.; formal analysis, B. A. and O. F.; investigation, S. S., K. I., and H. X.; resources, B. A. and O. F.; writing—original draft preparation, K. I. and S. S.; writing—review and editing, B. A. and O. F.; supervision, B. A. and O. F.; project administration, B. A. and O. F.; funding acquisition, B. A. and O. F. All authors have read and agreed to the published version of the manuscript.

Conflicts of interest

There are no conflicts to declare.

Acknowledgements

B. A. would like to thank the Kuwait Foundation for the Advancement of Sciences (KFAS, project number: PN18-14SC-01) for partially supporting this work. O. K. F. acknowledges the support from the U.S. Department of Energy (DOE) Office of Science, Basic Energy Sciences Program for separation (DE-FG02-08ER15967). This work made use of the EPIC facility of Northwestern University's NUANCE Center, which has received support from the Soft and Hybrid Nanotechnology Experimental (SHyNE) Resource (NSF ECCS-1542205), the MRSEC program (NSF DMR-1720139) at the Materials Research Center, the International Institute for Nanotechnology (IIN), the Keck Foundation, and the State of Illinois, through the IIN. This work made use of the IMSERC at Northwestern University, which has received support from the Soft and Hybrid Nanotechnology Experimental (SHyNE) Resource (NSF ECCS-1542205), the State of Illinois, and the International Institute for Nanotechnology (IIN).

Notes and references

1 F. Chen, H. F. Drake, F. Liang, J. A. Powell, W. Kun-Yu, Y. Tian-Hao and Z. Hong-Cai, Metal–Organic Frameworks as Versatile Platforms for Organometallic Chemistry, *Inorganics*, 2021, **9**, 27, DOI: **10.3390/inorganics9040027**.

2 L. Jiao, J. Y. R. Seow, W. S. Skinner, Z. U. Wang and H.-L. Jiang, Metal–organic frameworks: Structures and functional applications, *Mater. Today*, 2019, **27**, 43–68, DOI: **10.1016/j.mattod.2018.10.038**.

3 V. Unnikrishnan, O. Zabihi, M. Ahmadi, Q. Li, P. Blanchard, A. Kiziltas and M. Naebe, Metal–organic framework structure–property relationships for high-performance multifunctional polymer nanocomposite applications, *J. Mater. Chem. A*, 2021, **9**, 4348–4378, DOI: **10.1039/D0TA11255K**.

4 X. Ye and D. Liu, Metal–Organic Framework UiO-68 and Its Derivatives with Sufficiently Good Properties and Performance Show Promising Prospects in Potential Industrial Applications, *Cryst. Growth Des.*, 2021, **21**, 4780–4804, DOI: **10.1021/acs.cgd.1c00460**.

5 G. Chakraborty, I.-H. Park, R. Medishetty and J. J. Vittal, Two-Dimensional Metal-Organic Framework Materials: Synthesis, Structures, Properties and Applications, *Chem. Rev.*, 2021, **121**, 3751–3891, DOI: **10.1021/acs.chemrev.0c01049**.

6 W. Gong, Y. Xie, T. D. Pham, S. Shetty, F. A. Son, K. B. Idrees, Z. Chen, H. Xie, Y. Liu and R. Q. Snurr, *et al.*, Creating Optimal Pockets in a Clathrochelate-Based Metal–Organic Framework for Gas Adsorption and Separation: Experimental and Computational Studies, *J. Am. Chem. Soc.*, 2022, **144**, 3737–3745, DOI: **10.1021/jacs.2c00011**.

7 C. Jiang, X. Wang, Y. Ouyang, K. Lu, W. Jiang, H. Xu, X. Wei, Z. Wang, F. Dai and D. Sun, Recent advances in metal–organic frameworks for gas adsorption/separation, *Nanoscale Adv.*, 2022, **4**, 2077–2089, DOI: **10.1039/D2NA00061J**.

8 Z. L. Ma, P. X. Liu, Z. Y. Liu, J. J. Wang, L. B. Li and L. Tian, A Thermally and Chemically Stable Copper(II) Metal–Organic Framework with High Performance for Gas Adsorption and Separation, *Inorg. Chem.*, 2021, **60**, 6550–6558, DOI: **10.1021/acs.inorgchem.1c00357**.

9 H. Wang, J. J. Mahle, T. M. Tovar, G. W. Peterson, M. G. Hall, J. B. DeCoste, J. H. Buchanan and C. J. Karwacki, Solid-Phase Detoxification of Chemical Warfare Agents using Zirconium-Based Metal Organic Frameworks and the Moisture Effects: Analyze via Digestion, *ACS Appl. Mater. Interfaces*, 2019, **11**, 21109–21116, DOI: **10.1021/acsami.9b04927**.

10 H.-Q. Yin and X.-B. Yin, Metal–Organic Frameworks with Multiple Luminescence Emissions: Designs and Applications, *Acc. Chem. Res.*, 2020, **53**, 485–495, DOI: **10.1021/acs.accounts.9b00575**.

11 S. Bhattacharya, W. W. Ayass, D. H. Taffa, T. Nisar, T. Balster, A. Hartwig, V. Wagner, M. Wark and U. Kortz, Polyoxopalladate-Loaded Metal–Organic Framework (POP@MOF): Synthesis and Heterogeneous Catalysis, *Inorg. Chem.*, 2020, **59**, 10512–10521, DOI: **10.1021/acs.inorgchem.0c00875**.

12 D. Yang and B. Gates, Catalysis by Metal Organic Frameworks: Perspective and Suggestions for Future Research, *ACS Catal.*, 2019, **9**(3), 1779–1798, DOI: **10.1021/acscatal.8b04515**.

13 D. Rambabu, A. E. Lakraychi, J. Wang, L. Sieuw, D. Gupta, P. Apostol, G. Chanteux, T. Goossens, K. Robeyns and A. Vlad, An Electrically Conducting Li-Ion Metal–Organic Framework, *J. Am. Chem. Soc.*, 2021, **143**, 11641–11650, DOI: **10.1021/jacs.1c04591**.

14 Y. Jiang, H. Zhao, L. Yue, J. Liang, T. Li, Q. Liu, Y. Luo, X. Kong, S. Lu and X. Shi, *et al.*, Recent advances in lithium-based batteries using metal organic frameworks as electrode

materials, *Electrochem. Commun.*, 2021, **122**, 106881, DOI: **10.1016/j.elecom.2020.106881**.

15 X. Liu, Y. Shan, S. Zhang, Q. Kong and H. Pang, Application of metal organic framework in wastewater treatment, *Green Energy Environ.*, 2022, DOI: **10.1016/j.gee.2022.03.005**, In Press.

16 X. Chen, Y. Zhuang, N. Rampal, R. Hewitt, G. Divitini, C. O'Keefe, X. Liu, D. Whitaker, J. Wills and R. Jugdaohsingh, *et al.*, Formulation of Metal–Organic Framework-Based Drug Carriers by Controlled Coordination of Methoxy PEG Phosphate: Boosting Colloidal Stability and Redispersibility, *J. Am. Chem. Soc.*, 2021, **143**, 13557–13572, DOI: **10.1021/jacs.1c03943**.

17 J.-Z. Gu, M. Wen, X. Liang, Z. Shi, M. Kirillova and A. Kirillov, Multifunctional Aromatic Carboxylic Acids as Versatile Building Blocks for Hydrothermal Design of Coordination Polymers, *Crystals*, 2018, **8**, 83, DOI: **10.3390/cryst8020083**.

18 M. N. Ahamad, M. S. Khan, M. Shahid and M. Ahmad, Metal organic frameworks decorated with free carboxylic acid groups: topology, metal capture and dye adsorption properties, *Dalton Trans.*, 2020, **49**, 14690–14705, DOI: **10.1039/D0DT02949A**.

19 J. Gu, M. Wen, X. Liang, Z. Shi, M. V. Kirillova and A. M. Kirillov, Multifunctional Aromatic Carboxylic Acids as Versatile Building Blocks for Hydrothermal Design of Coordination Polymers, *Crystals*, 2018, **8**(2), 83, DOI: **10.3390/cryst8020083**.

20 A. Karmakar and I. Goldberg, Coordination polymers of flexible tetracarboxylic acids with metal ions. I. Synthesis of CH2- and (CH2)2-spaced bis(oxy)isophthalic acid ligands, and structural characterization of their polymeric adducts with lanthanoid ions, *CrystEngComm*, 2011, **13**, 339–349, DOI: **10.1039/C0CE00474J**.

21 D. Alezi, J. Jia, P. M. Bhatt, A. Shkurenko, V. Solovyeva, Z. Chen, Y. Belmabkhout and M. Eddaoudi, Reticular Chemistry for the Construction of Highly Porous Aluminum-Based nia-Metal–Organic Frameworks, *Inorg. Chem.*, 2022, **61**, 10661–10666, DOI: **10.1021/acs.inorgchem.2c00756**.

22 T. He, X.-J. Kong, J. Zhou, C. Zhao, K. Wang, X.-Q. Wu, X.-L. Lv, G.-R. Si, J.-R. Li and Z.-R. Nie, A Practice of Reticular Chemistry: Construction of a Robust Mesoporous Palladium Metal–Organic Framework via Metal Metathesis, *J. Am. Chem. Soc.*, 2021, **143**, 9901–9911, DOI: **10.1021/jacs.1c04077**.

23 S. Wuttke, Introduction to Reticular Chemistry. Metal–Organic Frameworks and Covalent Organic Frameworks By Omar M. Yaghi, Markus J. Kalmutzki, and Christian S. Diercks, *Angew. Chem., Int. Ed.*, 2019, **58**, 14024.

24 C. Gropp, S. Canossa, S. Wuttke, F. Gándara, Q. Li, L. Gagliardi and O. M. Yaghi, Standard Practices of Reticular Chemistry, *ACS Cent. Sci.*, 2020, **6**, 1255–1273, DOI: **10.1021/acscentsci.0c00592**.

25 V. Guillerm and M. Eddaoudi, The Importance of Highly Connected Building Units in Reticular Chemistry: Thoughtful Design of Metal–Organic Frameworks, *Acc. Chem. Res.*, 2021, **54**, 3298–3312, DOI: **10.1021/acs.accounts.1c00214**.

26 P. Chen, X. He, M. Pang, X. Dong, S. Zhao and W. Zhang, Iodine Capture Using Zr-Based Metal–Organic Frameworks (Zr-MOFs): Adsorption Performance and Mechanism, *ACS Appl. Mater. Interfaces*, 2020, **12**, 20429–20439, DOI: **10.1021/acsami.0c02129**.

27 H. Kim, D. Kim, D. Moon, Y. N. Choi, S. B. Baek and M. S. Lah, Symmetry-guided syntheses of mixed-linker Zr metal–organic frameworks with precise linker locations, *Chem. Sci.*, 2019, **10**, 5801–5806, DOI: **10.1039/C9SC01301F**.

28 C. Ardila-Suárez, J. Rodríguez-Pereira, V. G. Baldovino-Medrano and G. E. Ramírez-Caballero, An analysis of the effect of zirconium precursors of MOF-808 on its thermal stability, and structural and surface properties, *CrystEngComm*, 2019, **21**, 1407–1415, DOI: **10.1039/C8CE01722K**.

29 H. Mieno, R. Kabe, M. D. Allendorf and C. Adachi, Thermally activated delayed fluorescence of a Zr-based metal–organic framework, *Chem. Commun.*, 2018, **54**, 631–634, DOI: **10.1039/C7CC08595H**.

30 F. Xiao, X. Hu, Y. Chen and Y. Zhang, Porous Zr-Based Metal-Organic Frameworks (Zr-MOFs)-Incorporated Thin-Film Nanocomposite Membrane toward Enhanced Desalination Performance, *ACS Appl. Mater. Interfaces*, 2019, **11**, 47390–47403, DOI: **10.1021/acsami.9b17212**.

31 H. Furukawa, F. Gándara, Y.-B. Zhang, J. Jiang, W. L. Queen, M. R. Hudson and O. M. Yaghi, Water Adsorption in Porous Metal–Organic Frameworks and Related Materials, *J. Am. Chem. Soc.*, 2014, **136**, 4369–4381, DOI: **10.1021/ja500330a**.

32 J. H. Cavka, S. Jakobsen, U. Olsbye, N. Guillou, C. Lamberti, S. Bordiga and K. P. Lillerud, A New Zirconium Inorganic Building Brick Forming Metal Organic Frameworks with Exceptional Stability, *J. Am. Chem. Soc.*, 2008, **130**, 13850–13851, DOI: **10.1021/ja8057953**.

33 Y. Bai, Y. Dou, L.-H. Xie, W. Rutledge, J.-R. Li and H.-C. Zhou, Zr-based metal–organic frameworks: design, synthesis, structure, and applications, *Chem. Soc. Rev.*, 2016, **45**, 2327–2367, DOI: **10.1039/C5CS00837A**.

34 X. Gao, B. Guo, C. Guo, Q. Meng, J. Liang and J. Liu, Zirconium-Based Metal–Organic Framework for Efficient Photocatalytic Reduction of CO2 to CO: The Influence of Doped Metal Ions, *ACS Appl. Mater. Interfaces*, 2020, **12**, 24059–24065, DOI: **10.1021/acsami.0c05631**.

35 G.-Y. Qiao, S. Yuan, J. Pang, H. Rao, C. T. Lollar, D. Dang, J.-S. Qin, H.-C. Zhou and J. Yu, Functionalization of Zirconium-Based Metal–Organic Layers with Tailored Pore Environments for Heterogeneous Catalysis, *Angew. Chem., Int. Ed.*, 2020, **59**, 18224–18228, DOI: **10.1002/anie.202007781**.

36 J. Zheng, M. Wu, F. Jiang, W. Su and M. Hong, Stable porphyrin Zr and Hf metal–organic frameworks featuring 2.5 nm cages: high surface areas, SCSC transformations and catalyses, *Chem. Sci.*, 2015, **6**, 3466–3470, DOI: **10.1039/C5SC00213C**.

37 J. Tang, P. Li, T. Islamoglu, S. Li, X. Zhang, F. A. Son, Z. Chen, M. R. Mian, S.-J. Lee and J. Wu, *et al.*, Micropore environment regulation of zirconium MOFs for instantaneous hydrolysis of an organophosphorus chemical, *Cell Rep. Phys. Sci.*, 2021, **2**, 100612, DOI: **10.1016/j.xcrp.2021.100612**.

38 K. Ma, M. C. Wasson, X. Wang, X. Zhang, K. B. Idrees, Z. Chen, Y. Wu, S.-J. Lee, R. Cao and Y. Chen, *et al.*, Near-instantaneous catalytic hydrolysis of organophosphorus nerve agents with zirconium-based MOF/hydrogel composites, *Chem Catal.*, 2021, **1**, 721–733, DOI: **10.1016/j.checat.2021.06.008**.

39 Y. Liu, A. J. Howarth, N. A. Vermeulen, S.-Y. Moon, J. T. Hupp and O. K. Farha, Catalytic degradation of chemical warfare agents and their simulants by metal-organic frameworks, *Coord. Chem. Rev.*, 2017, **346**, 101–111, DOI: **10.1016/j.ccr.2016.11.008**.

40 J.-X. Wang, J. Yin, O. Shekhah, O. M. Bakr, M. Eddaoudi and O. F. Mohammed, Energy Transfer in Metal–Organic Frameworks for Fluorescence Sensing, *ACS Appl. Mater. Interfaces*, 2022, **14**, 9970–9986, DOI: **10.1021/acsami.1c24759**.

41 A. M. Plonka, Q. Wang, W. O. Gordon, A. Balboa, D. Troya, W. Guo, C. H. Sharp, S. D. Senanayake, J. R. Morris and C. L. Hill, *et al.*, In Situ Probes of Capture and Decomposition of Chemical Warfare Agent Simulants by Zr-Based Metal Organic Frameworks, *J. Am. Chem. Soc.*, 2017, **139**, 599–602, DOI: **10.1021/jacs.6b11373**.

42 Z. Chen, K. B. Idrees, S. Shetty, H. Xie, M. C. Wasson, W. Gong, X. Zhang, B. Alameddine and O. K. Farha, Regulation of Catenation in Metal–Organic Frameworks with Tunable Clathrochelate-Based Building Blocks, *Cryst. Growth Des.*, 2021, **21**, 6665–6670, DOI: **10.1021/acs.cgd.1c01151**.

43 M. Marmier, M. D. Wise, J. J. Holstein, P. Pattison, K. Schenk, E. Solari, R. Scopelliti and K. Severin, Carboxylic Acid Functionalized Clathrochelate Complexes: Large, Robust, and Easy-to-Access Metalloligands, *Inorg. Chem.*, 2016, **55**, 4006–4015, DOI: **10.1021/acs.inorgchem.6b00276**.